MOLECULAR DYNAMICS

Observation and ultrafast dynamics of a nonvalence correlation-bound state of an anion

James N. Bull[1,2] and Jan R. R. Verlet[1]*

Nonvalence states of molecular anions play key roles in processes, such as electron mobility, in rare-gas liquids, radiation-induced damage to DNA, and the formation of anions in the interstellar medium. Recently, a class of nonvalence bound anion state has been predicted by theory in which correlation forces are predominantly responsible for binding the excess electron. We present a direct spectroscopic observation of this nonvalence correlation-bound state (CBS) in the *para*-toluquinone trimer cluster anion. Time-resolved photoelectron velocity map imaging shows that photodetachment of the CBS produces a narrow and highly anisotropic photoelectron distribution, consistent with detachment from an s-like orbital. The CBS is bound by ~50 meV and decays by vibration-mediated autodetachment with a lifetime of 700 ± 100 fs. These states are likely to be common in large and/or polarizable anions and clusters and may act as doorway states in electron attachment processes.

INTRODUCTION

Unlike valence molecular orbitals that define molecular structure and bonding, nonvalence states are bound by long-range interactions between the molecular core and an electron and have little influence on molecular structure. These states are often weakly bound and have a highly diffuse orbital. For neutral atoms and molecules, the long-range Coulomb potential between a cation core and an electron forms the well-known Rydberg states (*1*). For molecular anions, the nonvalence binding interaction is between the neutral core and an excess electron. In the absence of the Coulomb interaction, much weaker dipole-electron forces can give rise to a dipole-bound state (*2*). These dipole-bound states play important roles in low-energy electron attachment processes leading to, for example, DNA damage (*3*, *4*) and astrochemical anion formation (*5*). However, many molecular systems do not have a sufficient dipole (or higher-order multipole) moment to support a dipole-bound state. Recently, high-level calculations on C_{60}^- (*6*–*9*), $C_6F_6^-$ (*10*), the coronene ($C_{24}H_{12}$) anion (*11*), and certain nitrile-containing anion conformations (*12*, *13*) show that correlation forces between the excess electron and the valence electrons of the molecular system can give rise to a nonvalence correlation-bound state (CBS). In these examples, electrostatic interactions alone are insufficient to bind the excess electron. The resulting state is weakly bound with a large fraction of its electron density extending beyond the van der Waals surface. This class of electronic state is closely related to image-potential states on metal or graphene surfaces (*14*, *15*) and superatom states of neutral fullerenes (*16*, *17*), and correlation forces are also essential in the binding of double Rydberg anions (*18*, *19*).

Correlation forces tend to be larger in highly polarizable systems, and calculations have predicted nonvalence CBSs for a number of cluster systems: $(NaCl)_n^-$ (n = 3 and 4) (*20*), $(C_6F_6)_2^-$ (*10*), $(C_{24}H_{12})_2^-$ (*11*), $(Xe)_n^-$ (n = 5 to 7) (*21*), $(NH_3)_6^-$ (*22*), and $(H_2O)_{24}^-$ (and likely other water cluster anions) (*23*, *24*). There is a belief that correlation forces are a key ingredient in defining the structure of solvated electrons (*25*) and controlling electron mobility in liquid Xe (*26*). To date, experimental evidence that correlation forces can bind an excess electron has come indirectly through the observation of $(Xe)_n^-$ (n = 6 and 7) by mass spectrometry in which the ground state is a nonvalence CBS (*21*, *27*), and from Rydberg electron transfer measurements on C_{60}, identifying near threshold s-wave electron attachment (*28*). However, the direct spectroscopic observation of a nonvalence CBS has remained elusive. A recent proposal suggested the use of ultrafast pump-probe experiments to create and monitor the dynamics of a CBS in real time (*7*), a strategy that we have recently applied to the formation of a dipole-bound state (*29*) and that was applied here to create, observe, and characterize a nonvalence CBS.

RESULTS

Our target system was the isolated *para*-toluquinone trimer cluster anion, $(pTQ)_3^-$, which was chosen because highly conjugated and cluster systems typically exhibit large correlation forces and are the likely systems to support a CBS. Gas-phase $(pTQ)_3^-$ was readily generated by electrospray ionization and transferred to vacuum, where a packet of its ions was selected by time-of-flight mass spectrometry. We used time-resolved photoelectron imaging for the spectroscopic identification and characterization of the nonvalence CBS. In our experiments, a femtosecond pump pulse at 3.10 eV (400 nm) photoexcited $(pTQ)_3^-$, and a second, delayed, femtosecond probe pulse at 1.55 eV (800 nm) monitored the evolution of the excited states. The photoelectron spectra and angular distributions provide direct insight into the binding energy and molecular orbital character of the transiently populated excited states. In principle, resonant excitation can directly access nonvalence states; however, in practice, oscillator strengths are weak relative to the excitation to valence excited states (*30*), and the requirement of narrow bandwidth lasers precludes direct characterization of their dynamical behavior.

Supporting computational work obtained equilibrium geometries of $(pTQ)_3^-$ and its closed-shell neutral, $(pTQ)_3$, as shown in Fig. 1 (A and B, respectively). The anion geometry exhibits two monomers (A1 and A2) that adopt a distorted π-stacked structure, with the third monomer (A3) acting as a side-on bridge. In the ground electronic state, the excess electron is almost exclusively (97%) localized on the A3 monomer. The molecular dipole moment at the anion and neutral geometries are 1.17 and 0.46 D, respectively, which are below the threshold of ~2.5 D required to experimentally support a dipole-bound state (*2*). Systematic electronic structure calculations of cluster geometries identified no low-energy cluster that could support a dipole-bound state (*29*). However, our calculations identified a nonvalence CBS that is

[1]Department of Chemistry, University of Durham, Durham DH1 3LE, U.K. [2]School of Chemistry, University of Melbourne, Parkville, Melbourne, Victoria 3010, Australia. *Corresponding author. Email: j.r.r.verlet@durham.ac.uk

bound by ~30 and ~100 meV in the anion and neutral geometries, respectively. The CBS is unbound within the Hartree-Fock approximation. The calculated natural orbital associated with the CBS at the neutral geometry is shown in Fig. 1C. The nonvalence CBS for $(pTQ)_3^-$ differs from those for high-symmetry systems, such as C_{60}^-, because the cluster has a residual dipole and quadrupole moment that can interact with the excess charge. Nevertheless, the dominant binding force for the nonvalence state of $(pTQ)_3^-$ is correlation.

To generate the CBS, we exploited the fact that there are several optically active π* resonances around $h\nu$ ~ 3.10 eV, which are quasi-bound states situated in the detachment continuum (*31*), and that their associated above-threshold nuclear dynamics induce coupling with the CBS. Figure 2A shows the photoelectron spectrum recorded at 3.10 eV, which is dominated by a distribution at low electron kinetic energy (eKE) that has some discernible vibrational structure. Figure 2B shows a selection of time-resolved photoelectron spectra in which a femtosecond pump pulse at 3.10 eV excites the π* resonance and a femtosecond probe pulse at 1.55 eV samples the excited-state population at time delay, *t*. The probe translates the transient (pumped) eKE distribution by the probe photon energy. Each time-resolved spectrum has the pump-only contribution ($t < 0$) subtracted, thus showing only the transient changes. The spectra in Fig. 2B show two time-resolved features: depletion of signal at low eKE and appearance of signal at high eKE. At delays near $t \sim 0$, the high-eKE appearance feature is broad and extends to ~2.2 eV, which is consistent with the adiabatic binding energy of $(pTQ)_3^-$ at 2.5 ± 0.2 eV. This broad feature evolves over the first 100 fs into a narrow peak centered at eKE = 1.50 eV, implying a binding energy of ~50 meV, although the resolution of the spectrometer is ~80 meV at this eKE. The inset in Fig. 2B shows the corresponding photoelectron image at a pump-probe delay of t = 150 fs. The narrow ring with a large radius that corresponds to the narrow peak in the spectra in Fig. 2B is highly anisotropic (β_2 ~ +1 for t > 100 fs), peaking along the laser polarization axis, ε. This anisotropy is consistent with p-wave photodetachment (*32*). Figure 2C shows the integrated photoelectron signal over the low-eKE depletion feature and over the high-eKE appearance feature. The integrated signals were fit with two exponential decays with lifetimes of $\tau_1 < 60$ fs (limited by cross-correlation) and τ_2 = 700 ± 100 fs. The faster τ_1 lifetime corresponds to the concerted development of the narrow anisotropic feature and the low-eKE depletion feature. The slower τ_2 lifetime corresponds to the concerted decay of the narrow peak and recovery of the low-eKE depletion feature. The fact that the integrated depletion signal is mirrored by the integrated appearance signal shows that the time-resolved decay dynamics are associated with the vibrational-structured low-eKE photoelectron feature in the single-photon spectrum (Fig. 2A).

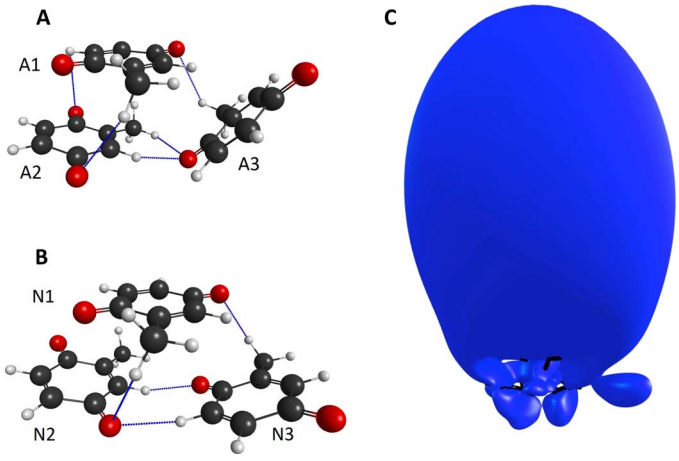

Fig. 1. Structure of the molecular cluster. The equilibrium anion (**A**) and neutral (**B**) geometries of the pTQ trimer. The blue dashed lines indicate hydrogen bonds responsible for cohesion of the cluster. (**C**) The natural orbital associated with the CBS at the neutral geometry.

DISCUSSION

We now turn to interpreting the time-resolved measurements. The initial broad high-eKE time-resolved feature shown in Fig. 2B, which is associated with lifetime τ_1, is consistent with photodetachment by the probe from the π* resonance, as illustrated in Fig. 3A. The large

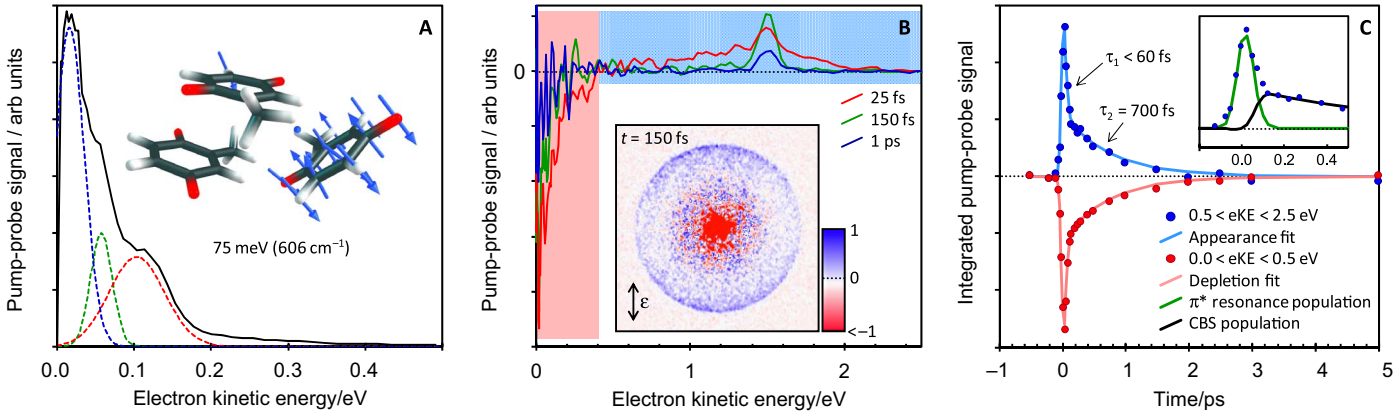

Fig. 2. Photoelectron imaging and dynamics of the CBS of $(pTQ)_3^-$. (**A**) The photoelectron spectrum taken at $h\nu$ = 3.10 eV with vibrational structure, together with an exemplary vibrational mode involving ring stretching and puckering that likely contributes to the vibrational structure. (**B**) Three examples of background-corrected time-resolved photoelectron spectra are shown. The inset shows the t = 150 fs velocity map image from which one of the spectra was derived and shows that the narrow high-eKE peak has an anisotropic angular distribution (β_2 ~ +1) that is parallel with the laser polarization vector, ε. (**C**) The integrated contributions of the low/high eKE features, as a function of pump-probe delay, *t*, show a fast and slow depletion/recovery that are assigned to internal conversion and autodetachment, respectively. The inset shows the fitted contribution of each relaxation pathway used to extract the lifetimes.

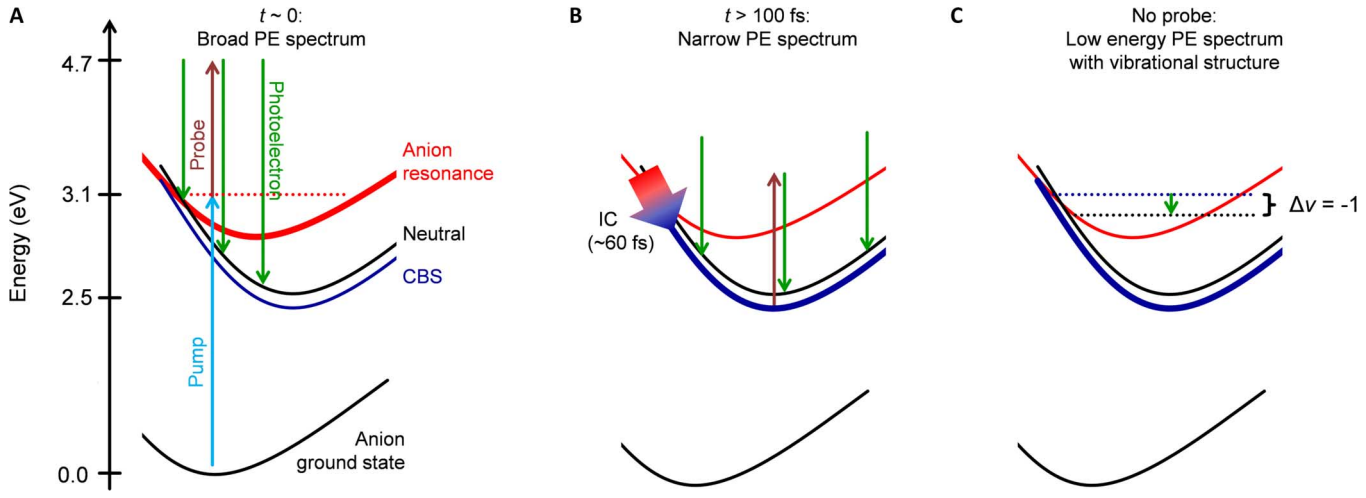

Fig. 3. Schematic illustration of the relaxation processes and photoelectron behavior following photoexcitation of $(pTQ)_3^-$. (**A**) The femtosecond pump pulse excites a π* resonance (t ~ 0) (bold line). The femtosecond probe pulse generates a broad distribution of photoelectrons (PEs) due to the difference between anion and neutral geometries. (**B**) Resonance population internally converts (τ_1 < 60 fs) to the nonvalence CBS (bold line). The photoelectron spectrum associated with the CBS is narrow because the CBS potential energy surface is nearly parallel to that of the neutral. (**C**) The CBS autodetaches (τ_2 = 700 ± 100 fs), mediated by specific vibrational modes of the cluster leading to the structured spectrum at low kinetic energy (Fig. 2A).

spectral width arises from differences in the ground and excited-state anion geometries (*29*, *33*, *34*). The narrow peak with an eKE distribution centered ~50 meV below the probe energy is consistent with an excited state of the anion that is weakly bound and has a potential energy surface that is parallel with the neutral ground-state potential energy surface (Fig. 3B). Furthermore, the photodetachment angular distribution (p-wave character) associated with the narrow peak implies that the orbital from which the electron was ejected has an s-like character. These three attributes are consistent with the narrow peak corresponding to photodetachment from a nonvalence excited state. Given that the cluster cannot support a dipole-bound state, the nonvalence excited state is the CBS identified in our calculations. Thus, the initial ultrafast lifetime (τ_1 < 60 fs) corresponds to the formation of the nonvalence CBS through internal conversion of the initially photoexcited π* resonance. The subsequent lifetime (τ_2 = 700 ± 100 fs) corresponds to the decay of the nonvalence CBS, and the mechanism can be assigned as autodetachment because the decay of the narrow peak is mirrored by the recovery of the depletion feature. Moreover, the apparent vibrational structure of the CBS autodetachment feature in the single-photon measurement (Fig. 2A) suggests that autodetachment is mediated by specific vibrational modes of the cluster.

The CBS dynamics described above are similar to the dipole-bound state formation and autodetachment dynamics recently characterized in π-stacked coenzyme Q_0 dimer anions (*29*). This similarity is not surprising considering the likeness in diffuse character between both types of nonvalence state. For the coenzyme Q_0 dimer anions, a photoelectron feature analogous to the low-eKE vibrational structure shown in Fig. 2A was assigned to autodetachment from the dipole-bound state facilitated by wagging and stretching modes of the carbonyl groups, which were highly excited in the initial photoexcitation. Drawing parallels with the present system, we assign the vibrational structure in Fig. 2A to result from vibrational-mediated autodetachment of the nonvalence CBS. That is, excited vibrational modes combined with monomer reorganization (motion of A3 to N3 in Fig. 1) modulate the CBS orbital to "shake off" the weakly bound electron. In this process, the electron is ejected with kinetic energy proportional to the vibrational mode frequencies in accordance with the Δv = −1 propensity rule (Fig. 3C) (*35*, *36*). Although this propensity rule is established for autodetachment from a dipole-bound state, it should be equally applicable to autodetachment from a nonvalence CBS. The associated vibrational structure in Fig. 2A can be empirically fitted with three Gaussian distributions; each Gaussian will probably have multiple contributing modes. Some of these modes may be those initially excited by the pump pulse, with a representative wagging mode shown in Fig. 2A. However, vibrational energy redistribution is likely to occur over the ~700-fs lifetime; other modes that are likely to contribute to Fig. 3C are those that are strongly coupled to the electron motion, such as the motion of N3 (Fig. 1B) (*35*). Unfortunately, a definitive assignment of the modes requires knowledge of the photoexcitation and internal conversion dynamics as well as potential energy surfaces for all states involved, which is not feasible for $(pTQ)_3^-$ at present.

The direct spectroscopic observation of a nonvalence state that is predominantly bound by correlation forces confirms the existence of this class of anion state. In accordance with theoretical studies, nonvalence CBS are likely to be common in a range of polarizable molecules and clusters. For example, correlation forces are expected to play a significant role in solvated electrons; these can be studied using cluster anions, which serve as proxies to investigate electron trapping in nanoscopic environments (*37*). In addition, given the observed similarity in the properties and dynamics of a nonvalence CBS and a dipole-bound state, processes associated with the latter should translate to systems with small or no dipole moments but that can support a nonvalence CBS. For example, the capture of a low-energy electron by a dipole-bound state is one of the primary mechanisms of interstellar anion formation (*5*). The same mechanistic argument of a large capture cross section for very low velocity electrons becomes applicable to large polyaromatic hydrocarbon or fullerene species that support a nonvalence CBS (*28*).

MATERIALS AND METHODS

The experimental setup has been described in detail elsewhere (*29*, *33*, *34*). Briefly, a ~2 mM solution of >99% purity *para*-toluquinone (Sigma-Aldrich) dissolved in analytical grade methanol was electrosprayed at −5 kV, and resulting anions were transferred via a vacuum transfer capillary into a radio frequency ring-electrode ion trap. Ions were thermalized to ~300 K in the trap, allowing formation of a statistical ensemble of cluster isomers. The trapped ions were unloaded into a colinear time-of-flight optics assembly in which the ion packet was accelerated along a 1.3-m flight region toward a continuous-mode penetrating field velocity-mapping assembly (*38*). Laser pulses were timed to interact with the mass-selected ion packet at the center of the velocity map imaging stack. Ejected electrons were velocity-mapped onto a dual (chevron) multichannel plate detector, followed by a P43 phosphor screen, which was monitored with a charge-coupled device camera. The eKE scale was calibrated from the spectrum of I^-, and the velocity-mapping resolution was ~5%. All velocity map image reconstructions used a polar onion-peeling algorithm (*39*), allowing the photoelectron spectrum and electron ejection angular distribution, β_2, to be obtained (*32*). All images were accumulated with a 500-ns multichannel plate gate.

Femtosecond laser pulses were derived from a Spectra-Physics Ti:Sapphire oscillator and regenerative amplifier. The 3.10-eV (400 nm; ~70 μJ) pump pulses were produced by frequency doubling of the 1.55-eV (800 nm) fundamental in a type I β-barium borate crystal. The 1.55-eV (~450 μJ) fundamental was used as the probe pulse. Pump and probe pulses were delayed relative to each other (t) using a motorized delay line. Both pulses were combined collinearly using a dichroic mirror and were loosely focused into the interaction region using a curved metal mirror. The pump-probe cross-correlation is ~60 fs, providing an ultimate time resolution of ~30 fs.

Supporting electronic structure calculations were performed using the Gaussian 09 (*40*), GAMESS-US (*41*), and CFOUR software packages (*42*). First, systematic PM6, ωB97XD//GEN1, and MP2//GEN1 geometry optimizations were performed on a range of $(pTQ)_3^-$ geometries to identify minimum energy structures (counterpoise-corrected) (*43*–*45*). The GEN1 basis set is the aug-cc-pVDZ basis set excluding the most diffuse set of d functions centered on carbon and oxygen atoms (*46*). All geometries were confirmed to represent geometrical minima through vibrational frequency analysis. The localized versus delocalized nature of the ground electronic state anion was determined from Mulliken (natural bond orbitals in parentheses) (*47*) charges and gave −0.03 (−0.01), 0.04 (−0.02), and −1.01 (−0.97) for A1, A2, and A3, respectively, indicating that the excess electron is localized on the A3 monomer.

Following protocol established in other theoretical studies of nonvalence CBS (*6*–*13*), the nonvalence CBS for $(pTQ)_3^-$ was characterized using the EA-EOM-CC2 method (*48*). EOM-MP2 and EOM-CC2 methods suffered numerical instabilities. CBS calculations required a set of 6s6p functions situated at the center of each pTQ ring (total of 720 spherical harmonic basis functions); EA-EOM-CC2/GEN1 (that is, no diffuse functions) failed to characterize a nonvalence CBS. Correlated virtual spaces were truncated to exclude the highest 300 orbitals (>50 eV in the Hartree-Fock approximation) for computational tractability.

Valence-localized π* resonances were characterized using multistate XMCQDPT2 theory with a (9, 12) CASSCF reference wave function (*49*). These calculations identified three resonances (oscillator strengths in parentheses), centered at 2.6 (0.02), 3.1 (0.001), and 3.4 (0.001) eV. Energies are expected to have an accuracy of ±0.2 eV (*29*, *34*).

SUPPLEMENTARY MATERIALS

Supplementary material for this article is available at http://advances.sciencemag.org/cgi/content/full/3/5/e1603106/DC1

Electron affinity determination

Comparison of the dynamics with $(CQ_0)_2^-$

Details of the π* resonances

Other cluster geometries

Multipole moments

fig. S1. $h\nu$ = 4.13 eV (300 nm) and $h\nu$ = 4.43 eV (270 nm) photoelectron spectra of pTQ_3^-.

fig. S2. CASSCF natural orbitals.

fig. S3. Geometries, relative energies, dipole moments, and Boltzmann populations of pTQ_3^- low-lying isomers.

fig. S4. Dipole moment vector of pTQ_3 minimum energy structure along with the natural orbital of the nonvalence state.

REFERENCES AND NOTES

1. R. F. Stebbings, F. B. Dunning, *Rydberg States of Atoms and Molecules* (Cambridge Univ. Press, 1983).
2. K. D. Jordan, F. Wang, Theory of dipole-bound anions. *Annu. Rev. Phys. Chem.* **54**, 367–396 (2003).
3. B. Boudaiffa, P. Cloutier, D. Hunting, M. A. Huels, L. Sanche, Resonant formation of DNA strand breaks by low-energy (3 to 20 eV) electrons. *Science* **287**, 1658–1660 (2000).
4. P. D. Burrow, G. A. Gallup, A. M. Scheer, Vibrational Feshbach resonances in uracil and thymine. *J. Chem. Phys.* **124**, 124310 (2006).
5. P. J. Sarre, The diffuse interstellar bands: A dipole-bound state hypothesis. *Mon. Not. R. Astron. Soc.* **313**, L14–L16 (2000).
6. V. K. Voora, L. S. Cederbaum, K. D. Jordan, Existence of a correlation bound *s*-type anion state of C_{60}. *J. Phys. Chem. Lett.* **4**, 849–853 (2013).
7. S. Klaiman, E. V. Gromov, L. S. Cederbaum, Extreme correlation effects in the elusive bound spectrum of C_{60}^-. *J. Phys. Chem. Lett.* **4**, 3319–3324 (2013).
8. V. G. Zakrzewski, O. Dolgounitcheva, J. V. Ortiz, Electron propagator calculations on the ground and excited states of C_{60}^-. *J. Phys. Chem. A* **118**, 7424–7429 (2014).
9. S. Klaiman, E. V. Gromov, L. S. Cederbaum, All for one and one for all: Accommodating an extra electron in C_{60}. *Phys. Chem. Chem. Phys.* **16**, 13287–13293 (2014).
10. V. K. Voora, K. D. Jordan, Nonvalence correlation-bound anion state of C_6F_6: Doorway to low-energy electron capture. *J. Phys. Chem. A* **118**, 7201–7205 (2014).
11. V. K. Voora, K. D. Jordan, Nonvalence correlation-bound anion states of polycyclic aromatic hydrocarbons. *J. Phys. Chem. Lett.* **6**, 3994–3997 (2015).
12. T. Sommerfeld, Multipole-bound states of succinonitrile and other dicarbonitriles. *J. Chem. Phys.* **121**, 4097 (2004).
13. T. Sommerfeld, K. M. Dreux, R. Joshi, Excess electrons bound to molecular systems with a vanishing dipole but large molecular quadrupole. *J. Phys. Chem. A* **118**, 7320–7329 (2014).
14. U. Höfer, I. L. Shumay, C. Reuß, U. Thomann, W. Wallauer, T. Fauster, Time-resolved coherent photoelectron spectroscopy of quantized electronic states on metal surfaces. *Science* **277**, 1480–1482 (1997).
15. V. M. Silkin, J. Zhao, F. Guinea, E. V. Chulkov, P. M. Echenique, H. Petek, Image potential states in graphene. *Phys. Rev. B* **80**, 121408 (2009).
16. M. Feng, J. Zhao, H. Petek, Atomlike, hollow-core–bound molecular orbitals of C_{60}. *Science* **320**, 359–362 (2008).
17. M. Feng, J. Zhao, T. Huang, X. Zhu, H. Petek, The electronic properties of superatom states of hollow molecules. *Acc. Chem. Res.* **44**, 360–368 (2011).
18. J. T. Snodgrass, J. V. Coe, C. B. Freidhoff, K. M. McHugh, K. H. Bowen, Photodetachment spectroscopy of cluster anions. Photoelectron spectroscopy of $H^-(NH_3)_1$, $H^-(NH_3)_2$ and the tetrahedral isomer of NH^-_4. *Faraday Discuss. Chem. Soc.* **86**, 241–256 (1988).
19. J. Simons, M. Gutowski, Double-Rydberg molecular anions. *Chem. Rev.* **91**, 669–677 (1991).
20. T. Sommerfeld, B. Bhattarai, V. P. Vysotskiy, L. S. Cederbaum, Correlation-bound anions of NaCl clusters. *J. Chem. Phys.* **133**, 114301 (2010).
21. V. G. Bezchastnov, V. P. Vysotskiy, L. S. Cederbaum, Anions of xenon clusters bound by long-range electron correlations. *Phys. Rev. Lett.* **107**, 133401 (2011).
22. T. Sommerfeld, Excess electrons bound to small ammonia clusters. *J. Phys. Chem. A* **112**, 11817–11823 (2008).
23. T. Sommerfeld, K. D. Jordan, Electron binding motifs of $(H_2O)_n^-$ clusters. *J. Am. Chem. Soc.* **128**, 5828–5833 (2006).
24. V. P. Vysotskiy, L. S. Cederbaum, T. Sommerfeld, V. K. Voora, K. D. Jordan, Benchmark calculations of the energies for binding excess electrons to water clusters. *J. Chem. Theory Comput.* **8**, 893–900 (2012).
25. L. Turi, P. J. Rossky, Theoretical studies of spectroscopy and dynamics of hydrated electrons. *Chem. Rev.* **112**, 5641–5674 (2012).
26. D. F. Coker, B. J. Berne, D. Thirumalai, Path integral Monte Carlo studies of the behavior of excess electrons in simple fluids. *J. Chem. Phys.* **86**, 5689 (1987).

27. H. Haberland, T. Kolar, T. Reiners, Negatively charged xenon atoms and clusters. *Phys. Rev. Lett.* **63**, 1219–1222 (1989).
28. J. M. Weber, M.-W. Ruf, H. Hotop, Rydberg electron transfer to C_{60} and C_{70}. *Z. Phys. D: At., Mol. Clusters* **37**, 351–357 (1996).
29. J. N. Bull, C. W. West, J. R. R. Verlet, Ultrafast dynamics of formation and autodetachment of a dipole-bound state in an open-shell π-stacked dimer anion. *Chem. Sci.* **7**, 5352–5361 (2016).
30. M. L. Theis, A. Candian, A. G. G. M. Tielens, T. J. Lee, R. C. Fortenberry, Electronically excited states of PANH anions. *Phys. Chem. Chem. Phys.* **17**, 14761–14772 (2015).
31. K. D. Jordan, P. D. Burrow, Temporary anion states of polyatomic hydrocarbons. *Chem. Rev.* **87**, 557–588 (1987).
32. R. N. Zare, Photoejection dynamics. *Mol. Photochem.* **4**, 1–37 (1972).
33. D. A. Horke, Q. Li, L. Blancafort, J. R. R. Verlet, Ultrafast above-threshold dynamics of the radical anion of a prototypical quinone electron-acceptor. *Nat. Chem.* **5**, 711–717 (2013).
34. J. N. Bull, C. W. West, J. R. R. Verlet, On the formation of anions: Frequency-, angle-, and time-resolved photoelectron imaging of the menadione radical anion. *Chem. Sci.* **6**, 1578–1589 (2015).
35. J. Simons, Propensity rules for vibration-induced electron detachment of anions. *J. Am. Chem. Soc.* **103**, 3971–3976 (1981).
36. D.-L. Huang, H.-T. Liu, C.-G. Ning, G.-Z Zhu, L.-S. Wang, Probing the vibrational spectroscopy of the deprotonated thymine radical by photodetachment and state-selective autodetachment photoelectron spectroscopy via dipole-bound states. *Chem. Sci.* **6**, 3129–3138 (2015).
37. R. M. Young, D. M. Neumark, Dynamics of solvated electrons in clusters. *Chem. Rev.* **112**, 5553–5577 (2010).
38. D. A. Horke, G. M. Roberts, J. Lecointre, J. R. R. Verlet, Velocity-map imaging at low extraction fields. *Rev. Sci. Instrum.* **83**, 063101 (2012).
39. G. M. Roberts, J. L. Nixon, J. Lecoitre, E. Wrede, J. R. R. Verlet, Toward real-time charged-particle image reconstruction using polar onion-peeling. *Rev. Sci. Instrum.* **80**, 053104 (2009).
40. M. J. Frisch, G. W. Trucks, H. B. Schlegel, G. E. Scuseria, M. A. Robb, J. R. Cheeseman, G. Scalmani, V. Barone, B. Mennucci, G. A. Petersson, H. Nakatsuji, M. Caricato, X. Li, H. P. Hratchian, A. F. Izmaylov, J. Bloino, G. Zheng, J. L. Sonnenberg, M. Hada, M. Ehara, K. Toyota, R. Fukuda, J. Hasegawa, M. Ishida, T. Nakajima, Y. Honda, O. Kitao, H. Nakai, T. Vreven, J. A. Montgomery Jr., J. E. Peralta, F. Ogliaro, M. Bearpark, J. J. Heyd, E. Brothers, K. N. Kudin, V. N. Staroverov, R. Kobayashi, J. Normand, K. Raghavachari, A. Rendell, J. C. Burant, S. S. Iyengar, J. Tomasi, M. Cossi, N. Rega, J. M. Millam, M. Klene, J. E. Knox, J. B. Cross, V. Bakken, C. Adamo, J. Jaramillo, R. Gomperts, R. E. Stratmann, O. Yazyev, A. J. Austin, R. Cammi, C. Pomelli, J. W. Ochterski, R. L. Martin, K. Morokuma, V. G. Zakrzewski, G. A. Voth, P. Salvador, J. J. Dannenberg, S. Dapprich, A. D. Daniels, Ö. Farkas, J. B. Foresman, J. V. Ortiz, J. Cioslowski, D. J. Fox, *Gaussian 09, Revision D.01* (Gaussian Inc., 2009).
41. M.W. Schmidt, K. K. Baldridge, J. A. Boatz, S. T. Elbert, M. S. Gordon, J. H. Jensen, S. Koseki, N. Matsunaga, K. A. Nguyen, S. Su, T. L. Windus, M. Dupuis, J. A. Montgomery Jr., General atomic and molecular electronic structure system. *J. Comput. Chem.* **14**, 1347–1363 (1993).
42. CFOUR, a quantum chemical program package written by J. F. Stanton, J. Gauss, M. E. Harding, P. G. Szalay with contributions from A. A. Auer, R. J. Bartlett, U. Benedikt, C. Berger, D. E. Bernholdt, Y. J. Bomble, L. Cheng, O. Christiansen, F. Engel, R. Faber, M. Heckert, O. Heun, C. Huber, T.-C. Jagau, D. Jonsson, J. Jusélius, K. Klein, W. J. Lauderdale, F. Lipparini, D. A. Matthews, T. Metzroth, L. A. Mück, D. P. O'Neill, D. R. Price, E. Prochnow, C. Puzzarini, K. Ruud, F. Schiffmann, W. Schwalbach, C. Simmons, S. Stopkowicz, A. Tajti, J. Vázquez, F. Wang, J. D. Watts and the integral packages *MOLECULE* (J. Almlöf and P.R. Taylor), *PROPS* (P. R. Taylor), *ABACUS* (T. Helgaker, H. J. Aa. Jensen, P. Jørgensen, and J. Olsen), and ECP routines by A. V. Mitin and C. van Wüllen. For the current version, see www.cfour.de.
43. J. J. P. Stewart, Optimization of parameters for semiempirical methods V: Modification of NDDO approximations, application to 70 elements. *J. Mol. Model.* **13**, 1173–1213 (2007).
44. J.-D. Chai, M. Head-Gordon, Long-range corrected hybrid density functionals with damped atom–atom dispersion corrections. *Phys. Chem. Chem. Phys.* **10**, 6615–6620 (2008).
45. S. F. Boys, F. Bernardi, The calculation of small molecular interactions by the differences of separate total energies. Some procedures with reduced errors. *Mol. Phys.* **19**, 553–566 (1970).
46. R.A. Kendall, T. H. Dunning Jr., R. J. Harrison, Electron affinities of the first-row atoms revisited. Systematic basis sets, wave functions. *J. Chem. Phys.* **96**, 6796–6806 (1992).
47. A. E. Reed, R. B. Weinstock, F. Weinhold, Natural population analysis. *J. Chem. Phys.* **83**, 735–746 (1985).
48. M. Nooijen, R. J. Bartlett, Equation of motion coupled cluster method for electron attachment. *J. Chem. Phys.* **102**, 3629 (1995).
49. A. A. Granovsky, Extended multi-configuration quasi-degenerate perturbation theory: The new approach to multi-state multi-reference perturbation theory. *J. Chem. Phys.* **134**, 214113 (2011).

Acknowledgments: We are grateful to T. Sommerfeld (Southeastern Louisiana University) for insightful discussions and C. West (Kyoto University) for laboratory assistance. **Funding:** This work was funded by the European Research Council under Starting Grant 306536. **Author contributions:** J.N.B. and J.R.R.V. conceived the experiment. J.N.B. conducted the experiments and calculations. J.N.B. and J.R.R.V. analyzed the data, discussed the results, and wrote the manuscript. **Competing interests:** The authors declare that they have no competing interests. **Data and materials availability:** All data needed to evaluate the conclusions in the paper are present in the paper and/or the Supplementary Materials. Additional data related to this paper may be requested from the authors.

Submitted 7 December 2016
Accepted 22 March 2017
Published 19 May 2017
10.1126/sciadv.1603106

Citation: J. N. Bull, J. R. R. Verlet, Observation and ultrafast dynamics of a nonvalence correlation-bound state of an anion. *Sci. Adv.* **3**, e1603106 (2017).

Science Advances
AAAS

Observation and ultrafast dynamics of a nonvalence correlation-bound state of an anion

James N. Bull and Jan R. R. Verlet (May 19, 2017)
Sci Adv 2017, 3:.
doi: 10.1126/sciadv.1603106